




eIF2 α incites photoreceptor cell and retina damage by all-*trans*-retinal

Received for publication, November 9, 2022, and in revised form, March 21, 2023. Published, Papers in Press, April 7, 2023.
<https://doi.org/10.1016/j.jbc.2023.104686>

Danxue He¹, Lei Tao¹, Binxiang Cai¹, Xiangjun Chen^{2,3} , Yan Wang⁴, Shiyong Li¹, Chunyan Liao¹, Yuling Chen¹, Jingmeng Chen⁵, Zuguo Liu^{1,*}, and Yalin Wu^{1,6,7,*}

From the ¹Fujian Provincial Key Laboratory of Ophthalmology and Visual Science, Fujian Engineering and Research Center of Eye Regenerative Medicine, Department of Ophthalmology, Xiang'an Hospital of Xiamen University, Eye Institute of Xiamen University, School of Medicine, Xiamen University, Xiamen, China; ²Eye Center of the Second Affiliated Hospital, and ³Institute of Translational Medicine, Zhejiang University School of Medicine, Hangzhou, China; ⁴Department of Ophthalmology, South China Hospital, Medical School, Shenzhen University, Shenzhen, China; ⁵School of Medicine, Xiamen University, Xiamen, China; ⁶Shenzhen Research Institute of Xiamen University, Shenzhen, China; ⁷Xiamen Eye Center of Xiamen University, School of Medicine, Xiamen University, Xiamen, China

Reviewed by members of the JBC Editorial Board. Edited by Kirill Martemyano

Dry age-related macular degeneration (AMD) and recessive Stargardt's disease (STGD1) lead to irreversible blindness in humans. The accumulation of all-*trans*-retinal (atRAL) induced by chaos in visual cycle is closely associated with retinal atrophy in dry AMD and STGD1 but its critical downstream signaling molecules remain ambiguous. Here, we reported that activation of eukaryotic translation initiation factor 2 α (eIF2 α) by atRAL promoted retinal degeneration and photoreceptor loss through activating c-Jun N-terminal kinase (JNK) signaling-dependent apoptosis and gasdermin E (GSDME)-mediated pyroptosis. We determined that eIF2 α activation by atRAL in photoreceptor cells resulted from endoplasmic reticulum homeostasis disruption caused at least in part by reactive oxygen species production, and it activated JNK signaling independent of and dependent on activating transcription factor 4 and the activating transcription factor 4/transcription factor C/EBP homologous protein (CHOP) axis. CHOP overexpression induced apoptosis of atRAL-loaded photoreceptor cells through activating JNK signaling rather than inhibiting the expression of antiapoptotic gene *Bcl2*. JNK activation by eIF2 α facilitated photoreceptor cell apoptosis caused by atRAL *via* caspase-3 activation and DNA damage. Additionally, we demonstrated that eIF2 α was activated in neural retina of light-exposed *Abca4*^{-/-}*Rdh8*^{-/-} mice, a model that shows severe defects in atRAL clearance and displays primary features of human dry AMD and STGD1. Of note, inhibition of eIF2 α activation by salubrinal effectively ameliorated retinal degeneration and photoreceptor apoptosis in *Abca4*^{-/-}*Rdh8*^{-/-} mice upon light exposure. The results of this study suggest that eIF2 α is an important target to develop drug therapies for the treatment of dry AMD and STGD1.

The metabolism of retinoids preserves standard status of the visual cycle and it is crucial for the health of retina (1, 2). In the course of normal retinoid metabolism, retina-specific ABC transporter 4 (ABCA4) carries all-*trans*-retinal (atRAL) from the inside to outside of photoreceptor disc membranes where all-*trans*-retinol dehydrogenase 8 (RDH8) catalyzes the reduction of atRAL to all-*trans*-retinol (also known as vitamin A), which reveals a critically important role of ABCA4 and RDH8 in eliminating free atRAL (2–5). Massive amounts of evidence have confirmed that autosomal recessive Stargardt's disease (STGD1) is a monogenic form of hereditary macular degeneration arising from mutations in the *Abca4* gene (6–8). Also, *Abca4*, the STGD1 gene, has been considered as a risk factor of dry age-related macular degeneration (AMD) rather than wet AMD (9–12). Although no mutations in the *RDH8* gene are found to be related with retinal diseases in humans, *Rdh8*^{-/-} mice display slowed reduction of atRAL to all-*trans*-retinol (13, 14). Studies in the past have demonstrated that mice with a knockout (KO) of *Abca4* and *Rdh8* genes (*Abca4*^{-/-}*Rdh8*^{-/-} mice) exhibit atRAL clearance disruption and lipofuscin accumulation and reproduce primary features of dry AMD and STGD1, such as the degeneration in photoreceptors and the retinal pigment epithelium (RPE) (14). Furthermore, exposure to bright light rapidly increases atRAL levels in the retina and accelerates photoreceptor atrophy and RPE degeneration in *Abca4*^{-/-}*Rdh8*^{-/-} mice (15–19). Taken together, these lines of evidence suggest that atRAL toxicity is closely bound up with the progression of retinal damage.

Endoplasmic reticulum (ER) is the site where protein folding and posttranslational modifications occur for secreted and membrane proteins (20, 21). Damage to ER function gives rise to an accumulation of unfolded or misfolded proteins in the ER lumen, thereby eliciting ER stress and the resulting unfolded protein response (UPR) (22). UPR serves as a protective mechanism for sustaining cellular homeostasis and it is responsible for attenuating protein translation

* For correspondence: Yalin Wu, yalinw@xmu.edu.cn; Zuguo Liu, zuguoliu@xmu.edu.cn.

eIF2 α promotes retinal degeneration

and increasing protein refolding or degradation (22, 23). Nevertheless, if ER stress is severe or prolonged, cells will undergo apoptosis after UPR fails to get rid of unfolded or misfolded proteins (22, 24). Binding immunoglobulin protein (BiP), also referred to as 78-kDa glucose-regulated protein, is a major ER chaperone and it maintains protein kinase RNA-like ER kinase (PERK) in a monomeric inactive conformation *via* binding to the ER luminal domain of PERK (25). The buildup of unfolded or misfolded proteins in the ER lumen evokes dissociation of BiP from PERK, leading to activation of the cytosolic domain in PERK *via* its oligomerization followed by autophosphorylation (26–28). Active PERK phosphorylates eukaryotic translation initiation factor 2 α (eIF2 α), which impedes general protein synthesis (29). Under persistent ER stress, however, eIF2 α phosphorylation incites the translation of activating transcription factor 4 (ATF4), resulting in apoptosis through inducing the expression of transcription factor C/EBP homologous protein (CHOP) (30).

As of yet, the mechanisms underlying involvement of ER stress in the development of dry AMD and STGD1 are still not very clear. In the present study, using mouse and *in vitro* cell culture models, we elucidate the role of eIF2 α , the cytoplasmic protein that can be activated as a result of ER stress, in causing retinal degeneration in retinopathies characterized by disrupted clearance of atRAL.

Results

atRAL activates ER stress-mediated PERK/eIF2 α /ATF4/CHOP signaling pathway in 661W photoreceptor cells

Cone photoreceptor cell line 661W is derived from a mouse retinal tumor (31) and it was employed as an *in vitro* model for studying retinal degeneration in this study. 661W photoreceptor cells were treated for 6 h with 5- μ M atRAL

throughout the study, as explained by our recently published article (17). Induction of BiP is a marker for ER stress (32). Analyses using quantitative real-time PCR (qRT-PCR) and Western blotting showed that atRAL significantly increased BiP expression at mRNA and protein levels in 661W photoreceptor cells (Fig. 1, A and B). Immunofluorescence staining revealed that protein levels of p-PERK were significantly enhanced in 661W photoreceptor cells exposed to atRAL (Fig. 1C). The eIF2 α /ATF4/CHOP signaling pathway functions downstream of PERK and its activation is a consequence of ER stress and is capable of evoking apoptotic cell death (30, 33). As expected, we observed that protein levels of p-eIF2 α and the expression of ATF4 and CHOP at mRNA and protein levels were remarkably elevated in atRAL-loaded 661W photoreceptor cells (Fig. 1, A and B). Moreover, we have previously shown evidence that apoptosis visibly occurs in 661W photoreceptor cells in response to atRAL (17). These results suggest that atRAL elicits photoreceptor cell apoptosis by activating ER stress-mediated PERK/eIF2 α /ATF4/CHOP signaling pathway.

Silence of eIF2 α gene reduces apoptosis of atRAL-loaded 661W photoreceptor cells via inhibiting activation of both c-Jun N-terminal kinase and CHOP signaling and alleviating DNA damage

The expression of eIF2 α in 661W photoreceptor cells was efficiently knocked down by eIF2 α -targeted siRNA, as evidenced by qRT-PCR and Western blotting (Fig. 2, A and B). As expected, silencing the eIF2 α gene resulted in a significant decline in protein levels of p-eIF2 α and the ratio of the p-eIF2 α /eIF2 α protein level in 661W photoreceptor cells exposed to atRAL (Fig. 2B). There is already compelling evidence that DNA damage as well as activation of c-Jun N-terminal kinase (JNK) or CHOP signaling is in close relation with

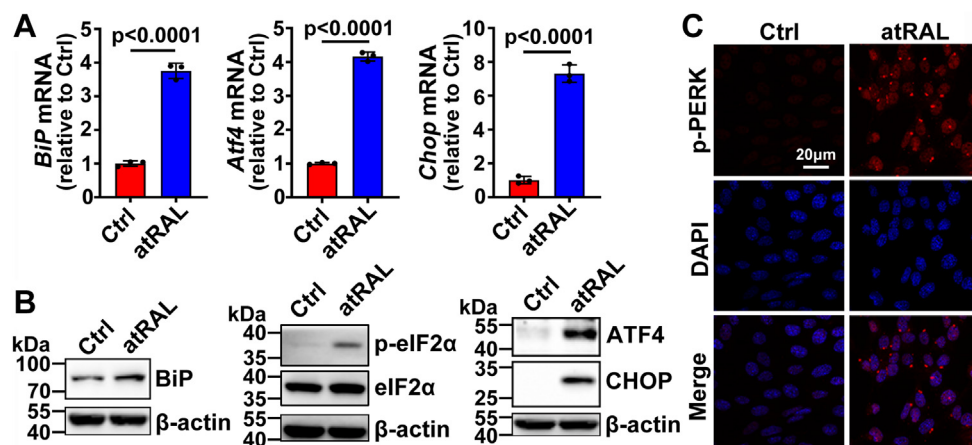


Figure 1. atRAL activates the PERK/eIF2 α /ATF4/CHOP signaling pathway of ER stress in 661W photoreceptor cells. **A**, qRT-PCR analysis of *BiP*, *Atf4*, and *Chop* genes in 661W photoreceptor cells incubated for 6 h with 5- μ M atRAL or DMSO (vehicle) alone. The mRNA levels of these genes were shown as fold changes relative to DMSO-treated controls. Statistical analyses were conducted by Student's *t* test. **B**, Western blots of BiP, p-eIF2 α , eIF2 α , ATF4, and CHOP in 661W photoreceptor cells exposed to 5- μ M atRAL or DMSO alone for 6 h. β -actin served as internal controls. Molecular-weight markers (kDa) are indicated to the left of the blots. **C**, immunofluorescence staining for p-PERK in 661W photoreceptor cells treated for 6 h with 5- μ M atRAL or DMSO alone. Nuclei were stained blue with DAPI. The scale bars represent 20 μ m. ATF4, activating transcription factor 4; atRAL, all-*trans*-retinal; DMSO, dimethyl sulfoxide; eIF2 α , eukaryotic translation initiation factor 2 α ; ER, endoplasmic reticulum; JNK, c-Jun N-terminal kinase; qRT-PCR, quantitative real-time PCR; PARP, poly ADP-ribose polymerase.

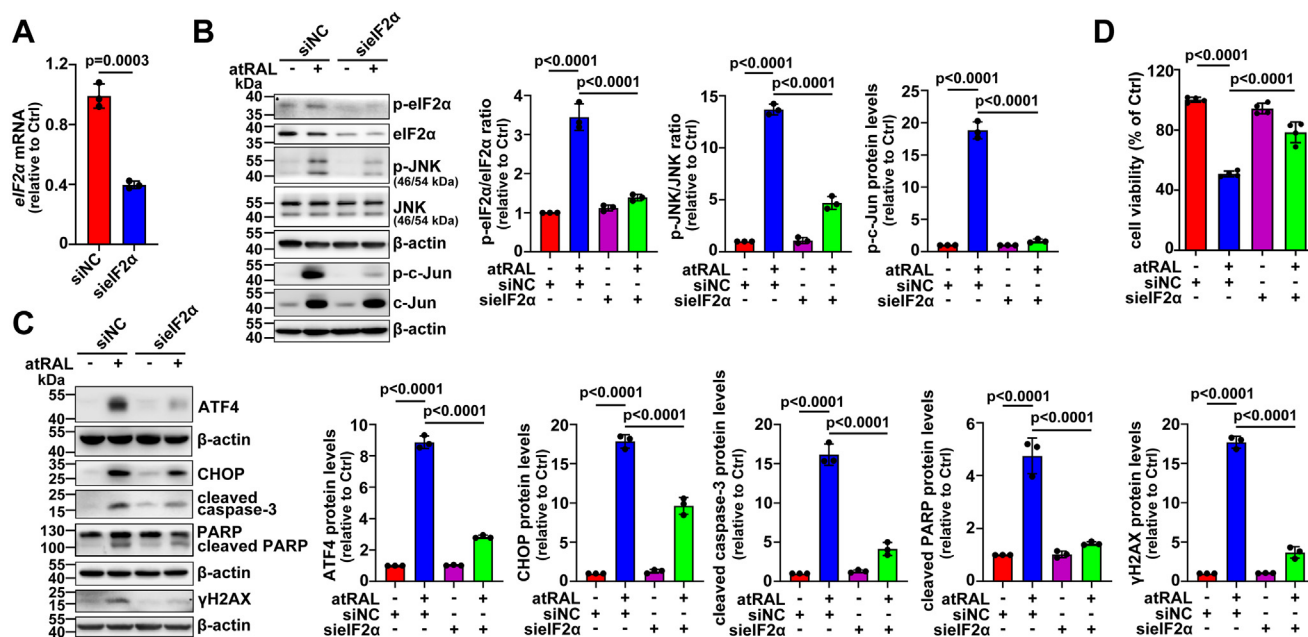


Figure 2. Knockdown of *eIF2α* inhibits *eIF2α*/ATF4/CHOP and JNK signaling pathways as well as caspase-3 activation and DNA damage in atRAL-loaded 661W photoreceptor cells and it enhances cellular survival. *A*, knockdown efficiency of *eIF2α* gene using a specific siRNA in 661W photoreceptor cells was evaluated by qRT-PCR. Cells transfected with *eIF2α* siRNA (si*eIF2α*) or negative control siRNA (siNC) were harvested at 24 h post-transfection. *Gapdh* was used as an internal control. *B*, Western blotting was used to examine protein levels of p-*eIF2α*, *eIF2α*, p-JNK, JNK, p-c-Jun, and c-Jun in si*eIF2α*- or siNC-transfected 661W photoreceptor cells incubated with 5- μ M atRAL and DMSO alone for 6 h, respectively. The blots of JNK displayed two bands having molecular weights of 46 and 54 kDa, which were assigned to JNK1 and JNK2, respectively (40). The ratios of p-*eIF2α*/*eIF2α* or p-JNK/JNK protein level and protein levels of p-c-Jun were shown as fold changes relative to DMSO-treated siNC controls. Levels of each protein were normalized to those of β -actin. The normalization for band intensity of p-*eIF2α*, *eIF2α*, p-JNK, or JNK against that of β -actin was individually made before calculating the ratios of p-*eIF2α*/*eIF2α* or p-JNK/JNK protein level. Note that band intensity of p-JNK or JNK was obtained as the sum of the intensity of two bands with molecular weights of 46 and 54 kDa. *C*, immunoblots of ATF4, CHOP, cleaved caspase-3, PARP, cleaved PARP, and γ H2AX in 661W photoreceptor cells that were transfected with siNC or si*eIF2α* for 24 h and then treated for 6 h with 5- μ M atRAL and DMSO alone, respectively. Protein levels of ATF4, CHOP, cleaved caspase-3, cleaved PARP, or γ H2AX were normalized to those of β -actin and presented as fold changes relative to DMSO-treated siNC controls. *D*, cell viability was detected by MTS assay. si*eIF2α*- or siNC-transfected 661W photoreceptor cells were exposed to 5- μ M atRAL and DMSO alone for 6 h, respectively. Student's *t* test in *A* and one-way ANOVA with Tukey's posttest in *B–D* were performed for statistical analyses. ATF4, activating transcription factor 4; atRAL, all-*trans*-retinal; DMSO, dimethyl sulfoxide; *eIF2α*, eukaryotic translation initiation factor 2 α ; JNK, c-Jun *N*-terminal kinase; PARP, poly ADP-ribose polymerase; qRT-PCR, quantitative real-time PCR.

apoptosis (30, 34, 35). c-Jun is a direct substrate of JNK and its elevated phosphorylation serves as an indicator of JNK activation (36). Poly ADP-ribose polymerase (PARP) is a substrate of caspase-3 and its cleavage reflects the execution of apoptosis by active caspase-3 (37). The formation of γ H2AX from phosphorylation of the Ser-139 residue of the histone variant H2AX is an early cellular response to the induction of DNA double-strand breaks and an increase in protein levels of γ H2AX denotes the onset of DNA damage (38). Immunoblot analysis revealed that the ratio of the p-JNK/JNK protein level and protein levels of p-JNK, p-c-Jun, ATF4, CHOP, cleaved caspase-3, cleaved PARP, and γ H2AX were clearly decreased in atRAL-loaded 661W photoreceptor cells with siRNA knockdown of *eIF2α* gene (Fig. 2, B and C). It should be mentioned here that the JNK kinase family consists of three isoforms, JNK1, JNK2, and JNK3, in which JNK1 and JNK2 are expressed in all tissues but JNK3 is only present in the brain, heart, and testes (39). The blots of JNK in Figure 2B showed two bands with molecular weights of 46 and 54 kDa, which corresponded to JNK1 and JNK2, respectively (40). Notably, the results of CellTiter 96 AQueous One Solution Cell Proliferation assay (MTS) disclosed that *eIF2α* knockdown visibly rescued 661W photoreceptor cells from the induction of

cytotoxicity by atRAL (Fig. 2D). These lines of evidence indicate that *eIF2α* activation by atRAL mediates apoptosis of photoreceptor cells through activating both JNK and CHOP signaling and triggering DNA damage.

Repressing *eIF2α* activation protects 661W photoreceptor cells from apoptosis induced by atRAL through attenuating JNK and CHOP signaling as well as DNA damage

Salubrinal (Sal) is a selective ER stress inhibitor that targets *eIF2α* (41). We observed the ability of 100- μ M Sal to clearly inhibit *eIF2α* phosphorylation and reduce the ratio of the p-*eIF2α*/*eIF2α* protein level in 661W photoreceptor cells upon atRAL exposure (Fig. 3A). Moreover, increases in protein levels of CHOP, p-JNK, p-c-Jun, c-Jun, cleaved caspase-3, cleaved PARP, and γ H2AX and the ratio of the p-JNK/JNK protein level in atRAL-loaded 661W photoreceptor cells were significantly prevented by Sal at the concentration of 100 μ M (Fig. 3, B–E). Importantly, after Sal treatment, 661W photoreceptor cells exposed to atRAL showed an increase of cell viability by approximately 18.3% (Fig. 3F). These data suggest that inactivation of *eIF2α* by Sal relieves photoreceptor cell apoptosis caused by atRAL *via* inhibiting both JNK and CHOP signaling and mitigating DNA damage.

eIF2 α promotes retinal degeneration

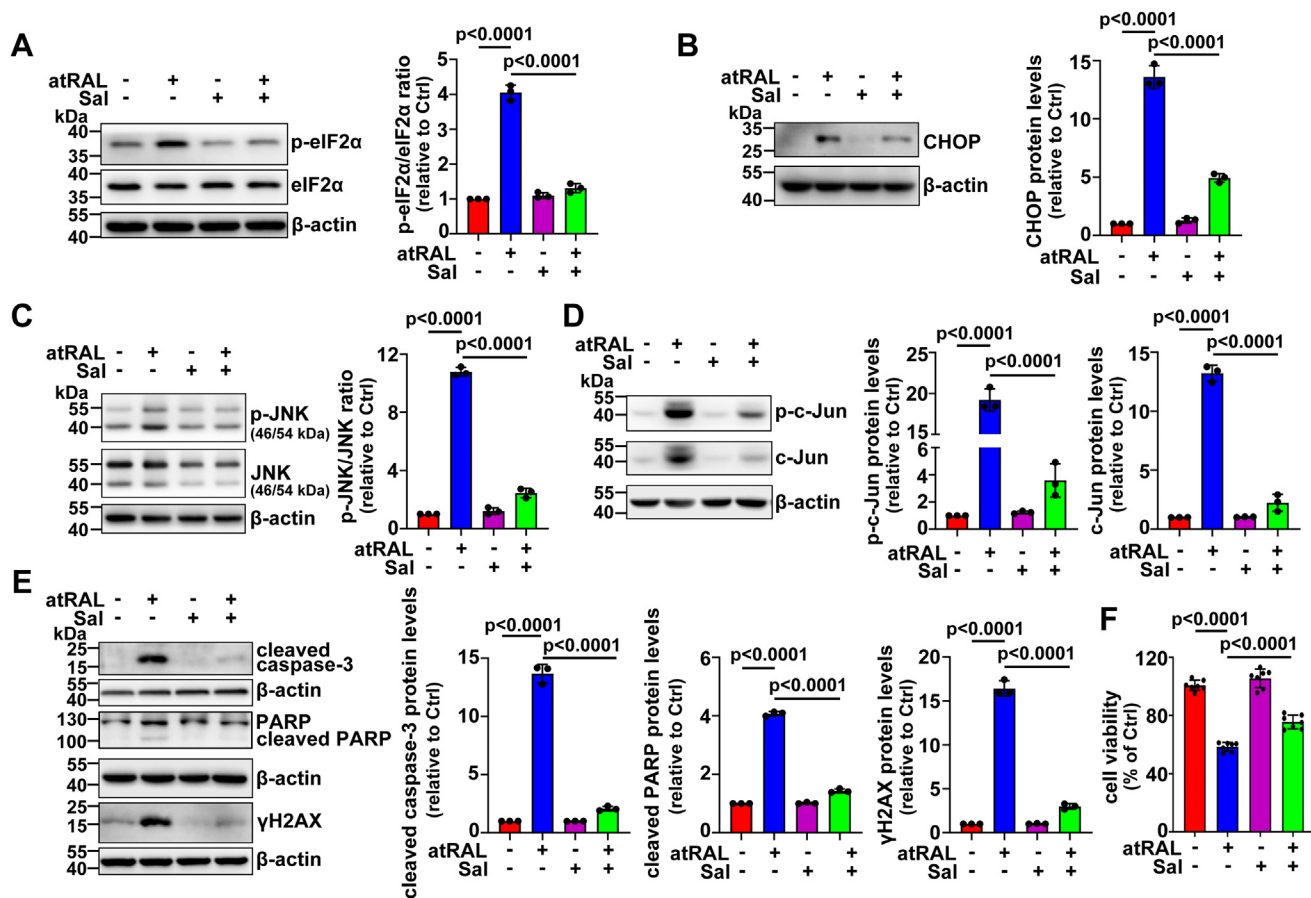


Figure 3. Sal that targets eIF2 α represses eIF2 α /CHOP and JNK signaling pathways as well as caspase-3 activation and DNA damage in atRAL-loaded 661W photoreceptor cells and it increases cell viability. A–E, Western blots of p-eIF2 α , eIF2 α , CHOP, p-JNK, JNK, p-c-Jun, c-Jun, cleaved caspase-3, PARP, cleaved PARP, and γ H2AX in 661W photoreceptor cells treated for 6 h with 5- μ M atRAL in the presence of 100- μ M Sal. Note that cells were pretreated with Sal for 2 h. Control cells were incubated with atRAL, Sal, or DMSO alone. The ratios of p-eIF2 α /eIF2 α or p-JNK/JNK protein level and protein levels of CHOP, p-c-Jun, c-Jun, cleaved caspase-3, cleaved PARP, and γ H2AX were expressed as fold changes relative to DMSO-treated controls. Levels of each protein were normalized to those of β -actin. The normalization for band intensity of p-eIF2 α , eIF2 α , p-JNK, or JNK against that of β -actin was individually made before calculating the ratios of p-eIF2 α /eIF2 α or p-JNK/JNK protein level. Note that band intensity of p-JNK or JNK was obtained as the sum of the intensity of two bands with molecular weights of 46 and 54 kDa. F, cytotoxicity was assessed by MTS assay. 661W photoreceptor cells were pretreated with 100- μ M Sal for 2 h and then incubated with 5- μ M atRAL for 6 h. Statistical analyses in A–F were conducted by one-way ANOVA with Tukey's posttest. atRAL, all-trans-retinal; DMSO, dimethyl sulfoxide; eIF2 α , eukaryotic translation initiation factor 2 α ; JNK, c-Jun N-terminal kinase; PARP, poly ADP-ribose polymerase.

Genetic deletion of Chop gene inhibits JNK signaling and cell death in atRAL-loaded 661W photoreceptor cells but it promotes eIF2 α phosphorylation

The results of Western blotting corroborated the absence of CHOP expression induced by atRAL in *Chop*^{-/-} compared to WT 661W photoreceptor cells (Fig. 4A). Knocking out the *Chop* gene led to a significant decrease in protein levels of p-JNK and p-c-Jun and the ratio of the p-JNK/JNK protein level in 661W photoreceptor cells in response to atRAL, and it evidently reversed damage to cellular morphology (Fig. 4, A and B). Cell viability following exposure to atRAL was up by 21.1% in *Chop*^{-/-} versus WT 661W photoreceptor cells (Fig. 4C). Interestingly, protein levels of p-eIF2 α and the ratio of the p-eIF2 α /eIF2 α protein level were found to be distinctly elevated in atRAL-loaded *Chop*^{-/-} compared to WT 661W photoreceptor cells (Fig. 4D), probably because CHOP KO inhibits activation of growth arrest and DNA damage-inducible protein 34 responsible for promoting ER client protein biosynthesis through dephosphorylating eIF2 α in

ER-stressed cells (42). In addition, it was further confirmed that protein expression of CHOP was obviously increased in the nucleus of 661W photoreceptor cells treated with 5- μ M atRAL for 6 h (Fig. 4E). These findings demonstrate that activation of CHOP by atRAL evokes apoptosis of photoreceptor cells, at least in part, through activating JNK signaling.

eIF2 α activates JNK signaling independent of CHOP in 661W photoreceptor cells in response to atRAL

To further ascertain the role of eIF2 α in activation of JNK signaling by atRAL, Sal and siRNA were used for impeding the activation of eIF2 α and the expression of eIF2 α or *Atf4* in *Chop*^{-/-} 661W photoreceptor cells, respectively. Treatment with 100- μ M Sal clearly decreased protein levels of p-eIF2 α , p-JNK, and p-c-Jun and the ratios of p-eIF2 α /eIF2 α or p-JNK/JNK protein level in *Chop*^{-/-} 661W photoreceptor cells exposed to atRAL and it resulted in an increase of 15.6% in cell viability (Fig. 5, A and B). Likewise, siRNA knockdown of eIF2 α remarkably reduced protein levels of p-eIF2 α , p-JNK,

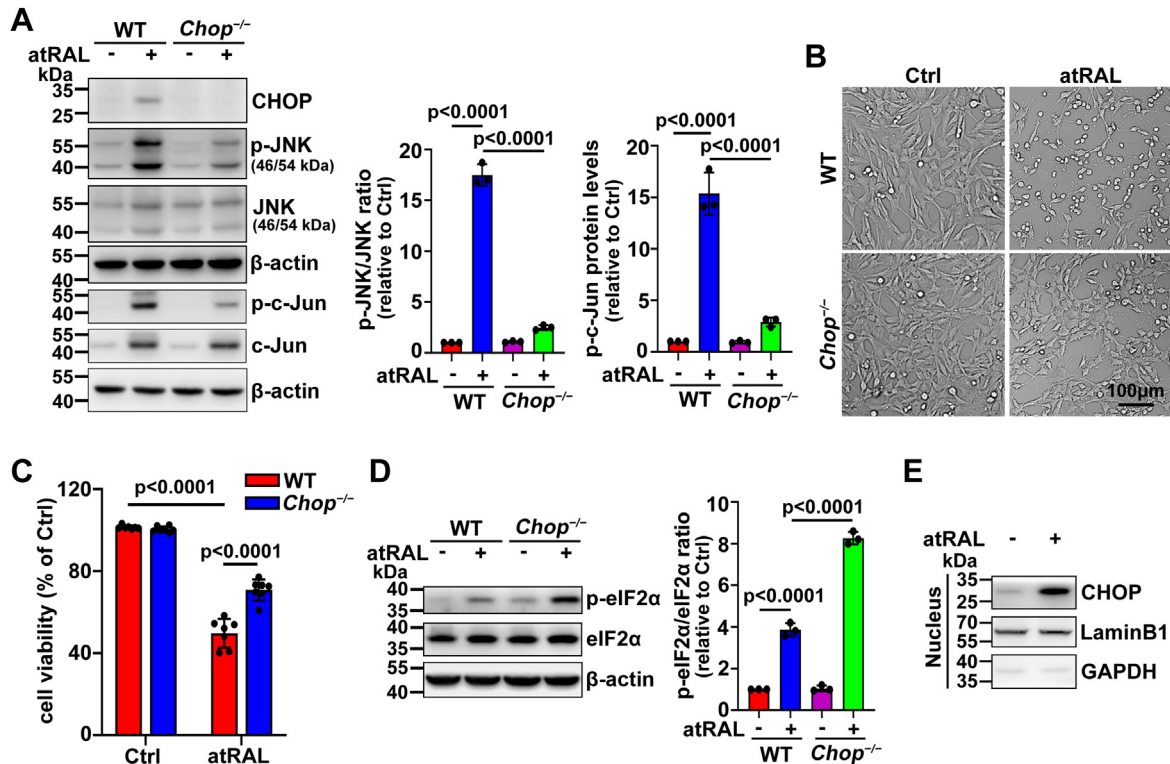


Figure 4. KO of *Chop* gene inhibits JNK signaling and the death in atRAL-loaded 661W photoreceptor cells but it promotes eIF2 α phosphorylation. **A**, immunoblots of CHOP, p-JNK, JNK, p-c-Jun, and c-Jun in WT or *Chop*^{-/-} 661W photoreceptor cells that were incubated for 6 h with 5- μ M atRAL and DMSO alone, respectively. The ratios of p-JNK/JNK protein level and protein levels of p-c-Jun were shown as fold changes relative to DMSO-treated WT controls. β -actin served as a loading control. **B**, cellular morphology was examined by a Leica DM2500 microscope. WT or *Chop*^{-/-} 661W photoreceptor cells were exposed for 6 h to 5- μ M atRAL and DMSO alone, respectively. The scale bars represent 100 μ m. **C**, cell viability, 6 h after exposure of WT, or *Chop*^{-/-} 661W photoreceptor cells to 5- μ M atRAL and DMSO alone, respectively, was evaluated by MTS assay. **D**, immunoblots of p-eIF2 α and eIF2 α in WT or *Chop*^{-/-} 661W photoreceptor cells treated for 6 h with 5- μ M atRAL and DMSO alone, respectively. The ratios of p-eIF2 α /eIF2 α protein level were shown as fold changes relative to DMSO-treated WT controls. **E**, Western blots of CHOP in the nucleus from WT 661W photoreceptor cells treated for 6 h with 5- μ M atRAL or DMSO alone. LaminB1 and GAPDH were used as internal controls. One-way ANOVA with Tukey's posttest in **A** and **D** and two-way ANOVA with Tukey's posttest in **C** were performed for statistical analyses. atRAL, all-trans-retinal; DMSO, dimethyl sulfoxide; eIF2 α , eukaryotic translation initiation factor 2 α ; JNK, c-Jun N-terminal kinase.

and p-c-Jun and the ratios of p-eIF2 α /eIF2 α or p-JNK/JNK protein level in atRAL-treated *Chop*^{-/-} 661W photoreceptor cells (Fig. 5C). Moreover, it was also observed that silencing of the *Atf4* gene resulted in a significant decline in protein levels of ATF4, p-JNK, and p-c-Jun as well as the ratio of the p-JNK/JNK protein level in *Chop*^{-/-} 661W photoreceptor cells upon exposure to atRAL (Fig. 5D). These data suggest that activation of eIF2 α by atRAL in photoreceptor cells is capable of activating JNK signaling in a CHOP-independent manner but it at least partially depends on ATF4.

Generation of reactive oxygen species by atRAL promotes ER stress-mediated activation of eIF2 α and CHOP signaling in 661W photoreceptor cells

After atRAL-loaded 661W photoreceptor cells were incubated with the reactive oxygen species (ROS) fluorescent probe 2',7'-dichlorodihydrofluorescein diacetate (H2DCFDA) and the ER-specific probe ER-Tracker Red, the localization of intracellular ROS to the ER were assessed by confocal laser-scanning microscopy. Exposure of 5- μ M atRAL to 661W photoreceptor cells for 6 h led to a dramatic elevation in the production of intracellular ROS (Fig. 6A). The green fluorescence-labeled ROS at a significant level in atRAL-loaded

661W photoreceptor cells was colocalized with the red fluorescence-labeled ER, as characterized by yellow fluorescence (Fig. 6A). We ever disclose that *N*-acetyl-L-cysteine (NAC), a potent ROS scavenger, markedly reduces the levels of ROS in atRAL-stimulated 661W photoreceptor cells at the concentration of 2 mM (17). In the current study, treatment with 2-mM NAC not only downregulated mRNA levels of *BiP* and *CHOP* but also decreased protein levels of p-eIF2 α and CHOP and the ratio of the p-eIF2 α /eIF2 α protein level in 661W photoreceptor cells after exposure to atRAL (Fig. 6, B and C). These results imply that ROS production caused by atRAL serves as an inducer of ER stress and functions upstream of eIF2 α and CHOP signaling in photoreceptor cells.

ER stress-mediated PERK/eIF2 α /CHOP signaling pathway is activated in neural retina of *Abca4*^{-/-}*Rdh8*^{-/-} mice upon light exposure

Forty-eight-h dark-adapted C57BL/6J and *Abca4*^{-/-}*Rdh8*^{-/-} mice were exposed for 2 h to 10,000-lx light emitting diode (LED) light and then raised in a dark room for 5 days, respectively. Our previous studies have indicated that, compared to light-free C57BL/6J mice, degeneration and apoptosis in photoreceptors and the RPE visibly occur in

eIF2 α promotes retinal degeneration

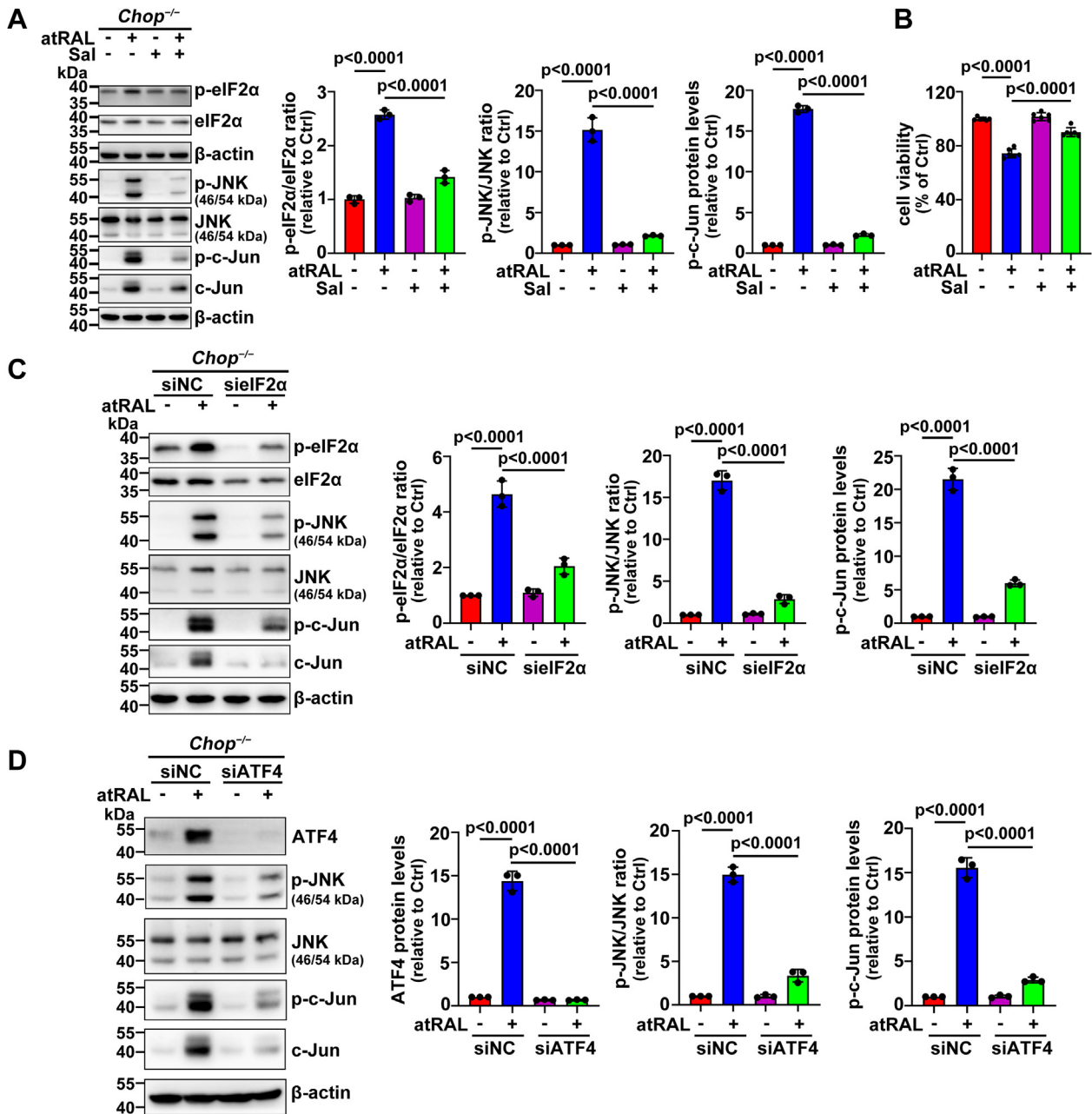


Figure 5. Activation of JNK signaling by eIF2 α occurs independent of CHOP in 661W photoreceptor cells in response to atRAL. *A*, Western blots of p-eIF2 α , eIF2 α , p-JNK, JNK, p-c-Jun, and c-Jun in Chop^{-/-} 661W photoreceptor cells that were pretreated with 100- μ M Sal for 2 h and then incubated for 6 h with 5- μ M atRAL. β -actin was used as an internal control. The ratios of p-eIF2 α /eIF2 α or p-JNK/JNK protein level and protein levels of p-c-Jun were presented as fold changes relative to DMSO-treated controls. *B*, cell viability was determined by MTS assay. Chop^{-/-} 661W photoreceptor cells were pretreated with 100- μ M Sal for 2 h and then exposed for 6 h to 5- μ M atRAL and DMSO alone, respectively. The ratios of p-eIF2 α /eIF2 α or p-JNK/JNK protein level and protein levels of p-c-Jun were shown as fold changes relative to DMSO-treated siNC controls. *C*, Western blots of p-eIF2 α , eIF2 α , p-JNK, JNK, p-c-Jun, and c-Jun in Chop^{-/-} 661W photoreceptor cells that were transfected with siNC or siEIF2 α for 24 h and then incubated for 6 h with 5- μ M atRAL and DMSO alone, respectively. The ratios of p-eIF2 α /eIF2 α or p-JNK/JNK protein level and protein levels of p-c-Jun were shown as fold changes relative to DMSO-treated siNC controls. *D*, immunoblots of ATF4, p-JNK, JNK, p-c-Jun, and c-Jun in Chop^{-/-} 661W photoreceptor cells that were transfected with siNC or siATF4 for 24 h and then exposed for 6 h to 5- μ M atRAL and DMSO alone, respectively. The ratios of p-JNK to JNK protein level and protein levels of ATF4 and p-c-Jun were shown as fold changes relative to DMSO-treated siNC controls. Statistical analyses in *A–D* were performed by one-way ANOVA with Tukey's posttest. atRAL, all-*trans*-retinal; DMSO, dimethyl sulfoxide; eIF2 α , eukaryotic translation initiation factor 2 α ; JNK, c-Jun N-terminal kinase.

Abca4^{-/-}*Rdh8*^{-/-} mice following exposure to light but they do not appear in light-free *Abca4*^{-/-}*Rdh8*^{-/-} mice and light-exposed C57BL/6J mice (17, 18). Using Western blot analysis, we observed a distinct elevation in protein levels of p-eIF2 α and CHOP and the ratio of p-eIF2 α to eIF2 α protein level as well as the expression of BiP in neural retina of *Abca4*^{-/-}*Rdh8*^{-/-} mice after light exposure (Fig. 7A). The

results of immunofluorescence staining revealed a significant elevation of p-PERK and CHOP protein levels in neuroretinal photoreceptors from light-exposed *Abca4*^{-/-}*Rdh8*^{-/-} mice (Fig. 7, B and C). These findings suggest that photoreceptor atrophy in mice characterized by compromised clearance of atRAL involves ER stress-mediated PERK/eIF2 α /CHOP signaling pathway.

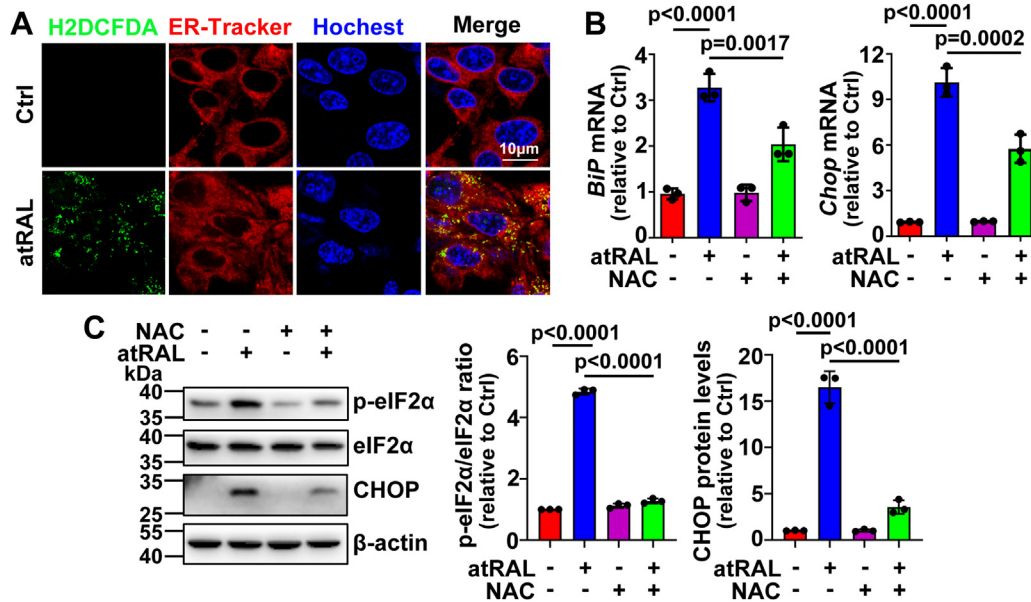


Figure 6. ROS induced by atRAL in 661W photoreceptor cells localizes in the ER and it facilitates ER stress-mediated activation of eIF2α and CHOP signaling. *A*, detection of the localization of ROS to the ER in atRAL-loaded 661W photoreceptor cells. After 661W photoreceptor cells were incubated for 6 h with 5-μM atRAL or DMSO alone, the localization of intracellular ROS to the ER was evaluated by costaining of H2DCFDA (green) with ER-Tracker Red. Nuclei were stained with Hoechst 33,342 (blue). Stained cells were observed by using the confocal fluorescence microscope. Colocalization of ROS and the ER is shown as yellow spots. The scale bars represent 10 μm. *B*, mRNA levels of *BiP* and *Chop* genes in 661W photoreceptor cells exposed for 6 h to 5-μM atRAL in the presence or absence of 2-mM ROS scavenger NAC. Note that cells were pretreated with 2-mM NAC for 2 h. *C*, Western blots of p-eIF2α, eIF2α, and CHOP in 661W photoreceptor cells that were pretreated for 2 h with 2-mM NAC and then incubated for 6 h with or without 5-μM atRAL. The ratios of p-eIF2α/eIF2α protein level and protein levels of CHOP were shown as fold changes relative to DMSO-treated controls. Levels of each protein were normalized to those of β-actin. The normalization for band intensity of p-eIF2α or eIF2α against that of β-actin was individually made before calculating the ratio of p-eIF2α/eIF2α protein level. Statistical analyses in *B* and *C* were carried out by one-way ANOVA with Tukey's posttest. atRAL, all-*trans*-retinal; BiP, binding immunoglobulin protein; DMSO, dimethyl sulfoxide; ER, endoplasmic reticulum; eIF2α, eukaryotic translation initiation factor 2α; H2DCFDA, 2',7'-dichlorodihydrofluorescein diacetate; NAC, *N*-acetyl-L-cysteine; ROS, reactive oxygen species.

Inhibition of eIF2α activation mitigates retinal degeneration and photoreceptor apoptosis in light-exposed *Abca4*^{-/-}*Rdh8*^{-/-} mice through inactivating JNK and CHOP signaling and repressing DNA damage

The results from the *Rpe65* gene sequencing analysis showed that *Abca4*^{-/-}*Rdh8*^{-/-} mice used in this study had a CTG (leucine) at codon 450 in the *Rpe65* gene (Fig. 8A). Histological analysis of neural retina by H&E staining indicated that both the degeneration of neuroretinal photoreceptors and the reduction of the thickness of photoreceptor outer nuclear layer in light-exposed *Abca4*^{-/-}*Rdh8*^{-/-} mice were significantly prevented by intraperitoneally injected Sal (8 mg/kg body weight) (Fig. 8, B and C). The results of TUNEL staining demonstrated that intraperitoneal treatment with Sal remarkably alleviated photoreceptor apoptosis in *Abca4*^{-/-}*Rdh8*^{-/-} mice upon light exposure (Fig. 8D). Consistent with the results of cell-based assays (Fig. 3A), Sal administration clearly decreased protein levels of p-eIF2α and the ratio of p-eIF2α/eIF2α protein level in extracts from neural retina of light-exposed *Abca4*^{-/-}*Rdh8*^{-/-} mice (Fig. 8E). Our recent studies have shown that activation of JNK signaling stimulates photoreceptor atrophy and apoptosis in *Abca4*^{-/-}*Rdh8*^{-/-} mice after exposure to light through a caspase-dependent mitochondrial pathway and DNA damage (17). In the current study, intraperitoneal injection of Sal dramatically reduced protein levels of p-JNK, p-c-Jun, γH2AX, and CHOP and the ratio of the p-JNK/JNK protein level in neural retina of *Abca4*^{-/-}*Rdh8*^{-/-} mice in response to light

exposure, as evidenced by Western blotting and immunofluorescence staining (Fig. 8, E–G). On examination by a small animal retinal imaging system, intraperitoneal administration of Sal effectively alleviated RPE degeneration in *Abca4*^{-/-}*Rdh8*^{-/-} mice exposed to light (Fig. 8H). Moreover, whole-mount immunofluorescence staining of the RPE with an anti-ZO-1 antibody also demonstrated that intraperitoneally injected Sal distinctly maintained tight junctions in the RPE of light-exposed *Abca4*^{-/-}*Rdh8*^{-/-} mice (Fig. 8I). These lines of evidence imply that eIF2α activation promotes retinal atrophy and photoreceptor apoptosis in mice with defects in atRAL clearance by activating JNK and CHOP signaling and triggering DNA damage.

Discussion

To date, there are only several lines of indirect evidence suggesting the involvement of ER stress in dry AMD (43–45). By contrast, to the best of our knowledge, there are no reports on the relationship of ER stress to STGD1. In this study, we utilized reliable animal and cell culture models characterized by the accumulation of atRAL for clarifying the effect of ER stress on dry AMD and STGD1 and its mechanisms. The results revealed that activation of eIF2α by ER stress promoted atRAL-induced photoreceptor apoptosis and retinal degeneration through activating JNK signaling in both CHOP-dependent and CHOP-independent manners.

eIF2 α promotes retinal degeneration

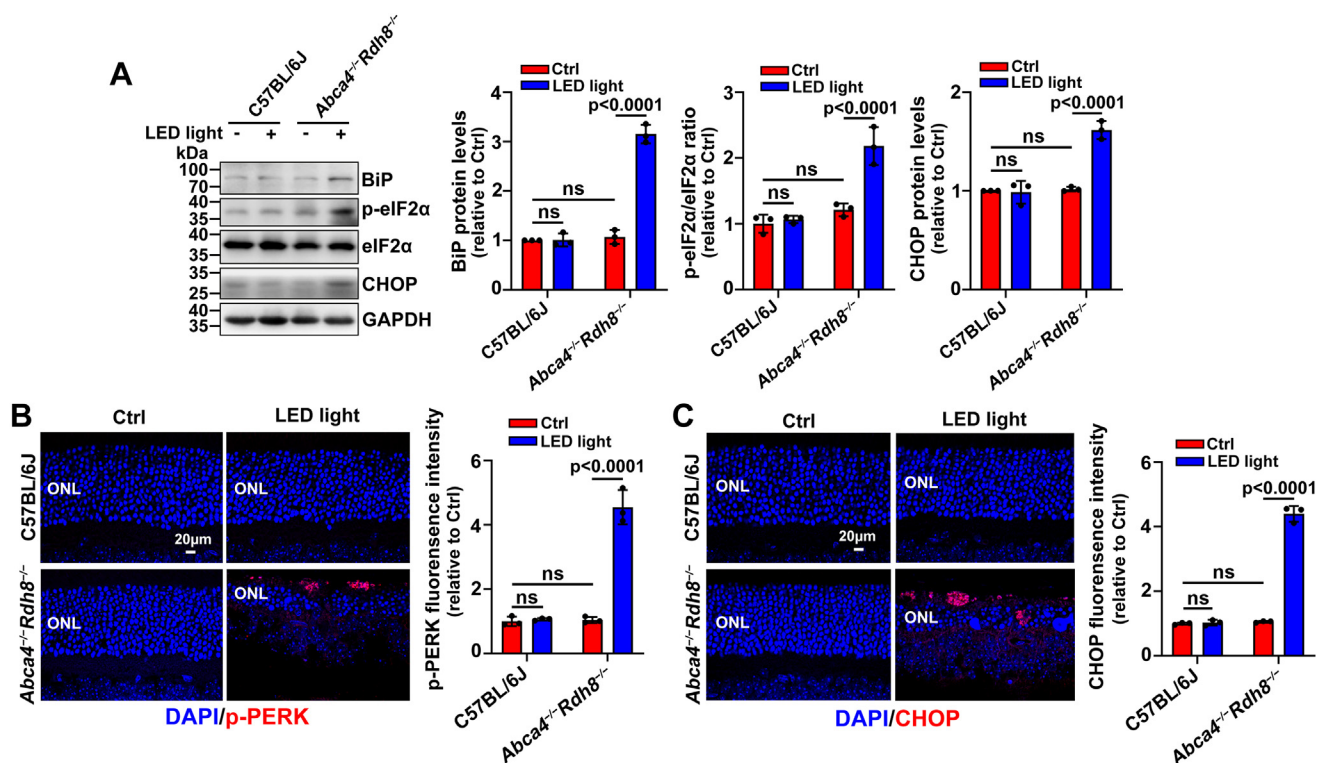


Figure 7. Exposure to LED light activates ER stress-mediated PERK/eIF2 α /CHOP signaling pathway in neural retina of *Abca4*^{-/-}*Rdh8*^{-/-} mice. C57BL/6J and *Abca4*^{-/-}*Rdh8*^{-/-} mice at 4 weeks of age were dark-adapted for 48 h and irradiated as we previously reported (17). Neural retinas were carefully dissected from eyeballs collected at day 5 after light exposure. **A**, Western blots of BiP, p-eIF2 α , eIF2 α , and CHOP in mouse neural retina. The band intensity for BiP, p-eIF2 α , eIF2 α , or CHOP was normalized to that for GAPDH. The ratios of p-eIF2 α /eIF2 α protein level and protein levels of BiP and CHOP were expressed as fold changes relative to light-free C57BL/6J mice. **B** and **C**, immunofluorescence staining for p-PERK (**B**) or CHOP (**C**) in mouse photoreceptors. Fluorescence intensity of p-PERK or CHOP was quantified by ImageJ software and shown as fold changes relative to light-free C57BL/6J mice. Results in **A–C** were from at least three mice per group. Statistical analyses in **A–C** were carried out with two-way ANOVA with Tukey's posttest. ns, not significant. BiP, binding immunoglobulin protein; ER, endoplasmic reticulum; eIF2 α , eukaryotic translation initiation factor 2 α ; LED, light emitting diode; ONL, outer nuclear layer; PERK, protein kinase RNA-like ER kinase; RDH8, retinol dehydrogenase 8.

Boyce and co-workers describe that Sal sustains eIF2 α phosphorylation in ER-stressed PC12 cells, a rat pheochromocytoma cell line (41). However, there is also a report on the ability of Sal to decrease protein levels of p-eIF2 α in ER-stressed C28/12 cells, a human chondrocyte cell line (46). Herein, we found that treatment with Sal significantly reduced protein levels of p-eIF2 α and the ratio of the p-eIF2 α /eIF2 α protein level in both atRAL-loaded 661W photoreceptor cells and neural retina of light-exposed *Abca4*^{-/-}*Rdh8*^{-/-} mice and it clearly enhanced cellular survival and alleviated retinal degeneration (Figs. 3, A and F and 8, B, C, E, H, and I). One possible explanation for the phenomenon is that reversal of tissue damage and cell viability loss relies on the ultimate role of Sal in relieving ER stress and subsequent eIF2 α phosphorylation. To further unravel the effect of Sal on the phosphorylation of eIF2 α , 661W photoreceptor cells were pretreated with 100- μ M Sal for 2 h and then incubated for 0.5, 1, 2, 3, and 6 h with 5- μ M atRAL or they were only exposed to 5- μ M atRAL for 0.5, 1, 2, 3, and 6 h. The data manifested that significant increases in the ratio of the p-eIF2 α /eIF2 α protein level and protein levels of p-eIF2 α were observed at 3 and 6 h but they were both prevented by Sal (Fig. S1). Moreover, the ratio of the p-eIF2 α /eIF2 α protein level and protein levels of p-eIF2 α in atRAL-loaded 661W photoreceptor cells reached

the highest values at 3 h but decreased by 30.31 and 9.21% at 6 h, respectively (Fig. S1). One possible explanation for this phenomenon is that CHOP activation by eIF2 α activates growth arrest and DNA damage-inducible protein 34 able to dephosphorylate eIF2 α (42).

We have previously reported that activation of JNK signaling by atRAL promotes apoptosis of 661W photoreceptor cells through the mitochondria-mediated caspase-dependent pathway and DNA damage induction (17). Although ROS production is a cause of JNK activation by atRAL in 661W photoreceptor cells (17), other factors that involve this event remain elusive. Recent studies have disclosed that increased expression of CHOP facilitates JNK activation (47). Indeed, we observed that elimination of the *Chop* gene clearly attenuated activation of JNK signaling by atRAL in 661W photoreceptor cells and it significantly ameliorated atRAL-induced cytotoxicity (Fig. 4, A–C). Given that activation of the eIF2 α /ATF4/CHOP axis by ER stress is capable of inducing apoptosis (30), we initially believed that eIF2 α evoked photoreceptor apoptosis triggered by atRAL only *via* CHOP-mediated JNK activation (Figs. 1 and 2). Interestingly, however, it was found that repression of eIF2 α activation by Sal or siRNA knockdown of the *eIF2 α* gene in *Chop*^{-/-} 661W photoreceptor cells distinctly mitigated activation of JNK

signaling by atRAL (Fig. 5, A and C), thus revealing that eIF2 α is also capable of activating JNK signaling without the help of CHOP in atRAL-loaded photoreceptor cells. To further clarify how eIF2 α activates JNK signaling in atRAL-loaded *Chop*^{-/-} 661W photoreceptor cells, we silenced the gene *Atf4* with siRNA, and found that ATF4 knockdown clearly repressed JNK signaling (Fig. 5D), which suggests that JNK activation by eIF2 α is achieved, at least in part, by ATF4 when CHOP is absent. Deletion of *Chop* gene resulted in a significant increase in phosphorylation of eIF2 α in 661W photoreceptor cells after atRAL exposure but it still clearly elevated cell viability (Fig. 4, C and D), thus revealing the importance of CHOP activation by eIF2 α in promoting photoreceptor cell death caused by atRAL. As we expected, silence of the *eIF2 α* gene or inhibition of eIF2 α activation by Sal visibly prevented caspase-3 activation and DNA damage in atRAL-loaded 661W photoreceptor cells and they both induced clear increases in cell viability (Figs. 2, C and D and 3, E and F).

It is reported that CHOP stimulates apoptosis *via* repressing the expression of antiapoptotic Bcl2 (48). We lately show that atRAL significantly decreases Bcl2 expression in 661W photoreceptor cells but a huge overexpression of Bcl2 almost does not affect the viability of 661W photoreceptor cells in response to atRAL (17). Conversely, knocking out *Jnk1* and *Jnk2* genes remarkably promotes the survival of atRAL-loaded 661W photoreceptor cells by inhibiting apoptotic cell death (17). Together these data reflect that CHOP mediates atRAL-induced apoptosis of 661W photoreceptor cells through activating JNK signaling rather than decreasing transcriptional levels of the gene *Bcl2* within the nucleus. In addition, it was important to point out that the atRAL concentration used in this study was of physiological significance, as we previously described (17).

A previous report indicates that the tendency for changes in c-Jun protein expression is consistent with that in protein levels of p-c-Jun (49). Indeed, protein levels of both c-Jun and p-c-Jun were decreased by Sal in atRAL-loaded 661W photoreceptor cells (Fig. 3D). By contrast, we observed that treatment with Sal downregulated protein levels of JNK in 661W photoreceptor cells incubated with and without atRAL, which is probably due to the ability of Sal to inhibit the synthesis of JNK protein.

We have previously presented evidence that the death of atRAL-loaded 661W photoreceptor cells and photoreceptor degeneration in light-exposed *Abca4*^{-/-}*Rdh8*^{-/-} mice involve ferroptosis and gasdermin E (GSDME)-mediated pyroptosis besides apoptosis (17–19) but they are unrelated to necroptosis (19). To evaluate the effect of eIF2 α on the induction of photoreceptor cell ferroptosis and pyroptosis by atRAL, the levels of N-terminal fragment of GSDME (GSDME-N), a direct executioner of pyroptosis, and ferrous ion (Fe²⁺), a required inducer of ferroptosis, in 661W photoreceptor cells transfected with negative control (NC) siRNA or eIF2 α siRNA (sieIF2 α) for 24 h and then incubated for 6 h with 5- μ M atRAL were examined by Western blotting and fluorescence staining with FeRhoNox-1, respectively. The results showed that

knockdown of eIF2 α by siRNA significantly reduced protein levels of GSDME-N in 661W photoreceptor cells in response to atRAL but it failed to decrease Fe²⁺ levels (Fig. S2), implying that eIF2 α activation by atRAL has the ability to promote pyroptotic cell death in photoreceptor cells yet it is incapable of inducing ferroptotic cell death.

Our previous report has shown that inhibiting JNK signaling distinctly alleviates photoreceptor atrophy in light-exposed *Abca4*^{-/-}*Rdh8*^{-/-} mice (17). In this article, repression of eIF2 α , upstream of JNK signaling, by intraperitoneal administration of Sal dramatically reversed damage to photoreceptors in *Abca4*^{-/-}*Rdh8*^{-/-} mice upon light exposure as well (Fig. 8, B–G). Immunofluorescence staining of neural retinas with antibodies specific for p-PERK, CHOP, and p-JNK revealed that ER stress and JNK activation did occur in photoreceptors of light-exposed *Abca4*^{-/-}*Rdh8*^{-/-} mice (Figs. 7, B and C and 8, F and G). In addition to relieving photoreceptor degeneration, intraperitoneally injected Sal also significantly ameliorated RPE atrophy and maintained RPE tight junctions in *Abca4*^{-/-}*Rdh8*^{-/-} mice following exposure to light (Fig. 8, H and I). Past studies in our laboratory using the human RPE cell line ARPE-19 indicate that RPE cell pyroptosis and apoptosis caused by atRAL are correlated with cleavage of GSDME and ER stress-mediated activation of the PERK/eIF2 α /ATF4/CHOP signaling pathway, respectively (45, 50). Most recently, we also show that JNK activation by atRAL stimulates apoptotic cell death and degeneration in the RPE of mice (51). Collectively, these lines of evidence suggest that activation of eIF2 α by atRAL should have a similar role in RPE and photoreceptor damage.

Based on the foregoing findings, a plausible mechanism was proposed for inducing photoreceptor and RPE cell death through the activation of eIF2 α by atRAL (Fig. 9). Intracellular atRAL disrupts ER homeostasis at least in part by the ROS production, leading to the accumulation of misfolded or unfolded proteins in ER lumen where they compete with PERK in binding to BiP. Upon BiP dissociation, PERK is oligomerized and autophosphorylated, which in turn phosphorylates eIF2 α in the cytosol. Active eIF2 α triggers the activation of JNK signaling independent of and dependent on ATF4 and the ATF4/CHOP axis. JNK activation mediates caspase-3 activation and DNA damage, finally resulting in apoptotic cell death. The active form of JNK (p-JNK) partially enters into the nucleus where it phosphorylates the histone H2AX to generate DNA damage indicator γ H2AX. Moreover, the ability of CHOP to induce apoptosis caused by atRAL is unrelated to the repression of antiapoptotic gene *Bcl2* expression. Alternatively, eIF2 α activation induces the cleavage of GSDME to produce GSDME-N that executes pyroptotic cell death. This is the first report that the activation of JNK signaling by eIF2 α does not require CHOP expression in cells upon exposure to stimuli. The results of this study identify eIF2 α as a key regulator of JNK signaling in association with retinal degeneration and photoreceptor/RPE cell death in retinopathies featured by disrupted clearance of atRAL. Pharmacological inhibition of eIF2 α may hold promises for the effective therapy of dry AMD and STGD1.

eIF2 α promotes retinal degeneration

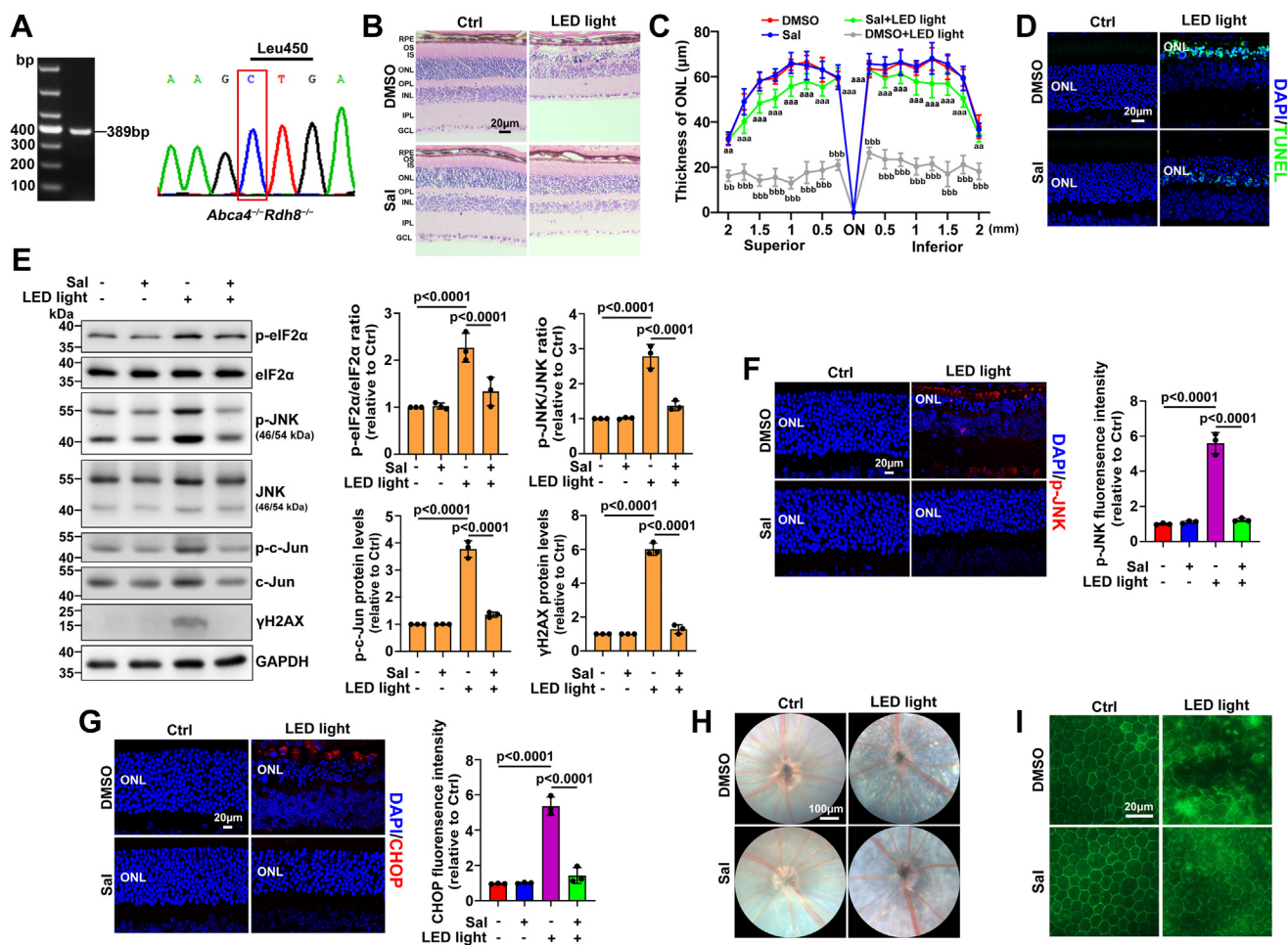


Figure 8. Intraperitoneal administration of Sal effectively ameliorates retinal degeneration and photoreceptor apoptosis through repressing activation of JNK signaling and CHOP by eIF2 α in light-exposed *Abca4*^{-/-}*Rdh8*^{-/-} mice. Four-week-old *Abca4*^{-/-}*Rdh8*^{-/-} mice were dark-adapted for 48 h, and then intraperitoneally injected with Sal or DMSO (vehicle) at a dose of 8 mg/kg body weight. Two hours later, the mice were exposed to 10,000-lx LED light for 2 h after their pupils were dilated with 1% tropicamide, followed by once-daily administration of Sal or DMSO in the dark for 4 days. Control *Abca4*^{-/-}*Rdh8*^{-/-} mice were intraperitoneally administered Sal or vehicle without exposure to light. **A**, genotyping of *Rpe65* gene variation in *Abca4*^{-/-}*Rdh8*^{-/-} mice. The 389-bp amplicon in the PCR corresponded to *Rpe65* gene. Gene sequencing disclosed that *Abca4*^{-/-}*Rdh8*^{-/-} mice used in this study had a CTG (leucine) at codon 450 in the *Rpe65* gene. **B**, the morphology of each mouse neural retina was examined by H&E staining. **C**, ONL thickness measurement on the Superior-Inferior meridian ($n = 9$). Two-way ANOVA with Bonferroni's multiple comparison test. ^{aa} $p < 0.01$, ^{aaa} $p < 0.001$ versus DMSO-treated light-exposed *Abca4*^{-/-}*Rdh8*^{-/-} mice; ^{bbb} $p < 0.01$, ^{bbb} $p < 0.001$ compared to DMSO-treated control *Abca4*^{-/-}*Rdh8*^{-/-} mice. **D**, apoptotic cells in mouse photoreceptors were analyzed by TUNEL staining. **E**, Western blots of p-eIF2 α , eIF2 α , p-JNK, JNK, p-c-Jun, c-Jun, and γ H2AX in extracts from each mouse neural retina. The ratios of p-eIF2 α /eIF2 α or p-JNK/JNK protein level and protein levels of p-c-Jun and γ H2AX were shown as fold changes relative to DMSO-treated control *Abca4*^{-/-}*Rdh8*^{-/-} mice. Levels of each protein were normalized to those of GAPDH. The normalization for band intensity of p-eIF2 α , eIF2 α , p-JNK, or JNK against that of GAPDH was individually made before calculating the ratios of p-eIF2 α /eIF2 α or p-JNK/JNK protein level. Note that band intensity of p-JNK or JNK was obtained as the sum of the intensity of two bands with molecular weights of 46 and 54 kDa. **F** and **G**, immunofluorescence staining of mouse photoreceptors with an anti-p-JNK antibody (**F**) or an anti-CHOP antibody (**G**). Fluorescence intensity of p-JNK or CHOP was quantified by ImageJ software and shown as fold changes relative to DMSO-treated control *Abca4*^{-/-}*Rdh8*^{-/-} mice. **H**, the RPE morphology of each mouse was visualized by a small animal retinal imaging system (Optoprobe; OPIMG-L). **I**, whole-mount ZO-1 (green) immunofluorescence staining of the mouse RPE was visualized by confocal microscopy. Results in **A**–**I** were from at least three mice per group. Statistical analyses in **E**–**G** were performed by one-way ANOVA with Tukey's posttest. The scale bars in **B**, **D**, **F**, **G**, and **I** represent 20 μ m. atRAL, all-trans-retinal; DMSO, dimethyl sulfoxide; eIF2 α , eukaryotic translation initiation factor 2 α ; JNK, c-Jun N-terminal kinase; LED, light emitting diode; RDH8, retinol dehydrogenase 8.

Experimental procedures

Reagents and antibodies

atRAL, 4',6-diamidino-2-phenylindole (DAPI), Hoechst 33,342, and Sal were obtained from Sigma-Aldrich. FerRho-Nox-1 was purchased from Goryo Chemical. TRleasy™ total RNA extraction reagent was obtained from Yeasen Corporation. ER-Tracker Red was purchased from Beyotime. NAC was obtained from Aladdin. Antibodies against cleaved caspase-3 (catalog no. 9664S), BiP (catalog no. 3177S), p-eIF2 α (catalog no. 3398S), eIF2 α (catalog no. 9722S), ATF4 (catalog no.

11815), CHOP (catalog no. 5554S), p-JNK (catalog no. 9255S), JNK (catalog no. 9252S), p-c-Jun (catalog no. 9261S), c-Jun (catalog no. 9165S), p-PERK (catalog no. 3179), PARP (catalog no. 9542S), β -actin (catalog no. 8457S), and GAPDH (catalog no. 5174S) were provided by Cell Signaling Technology. Anti-GSDME (catalog no. ab215191) was obtained from Abcam. Mouse anti- γ H2AX (catalog no. 05-636) was purchased from Millipore. Genomic DNA kit (catalog no. DP304-03) was purchased from TIANGEN. Mouse ZO-1 monoclonal antibody (catalog no. 33-9100), and Alexa Fluor 488-conjugated donkey anti-mouse (catalog no. A21202) and 594-conjugated

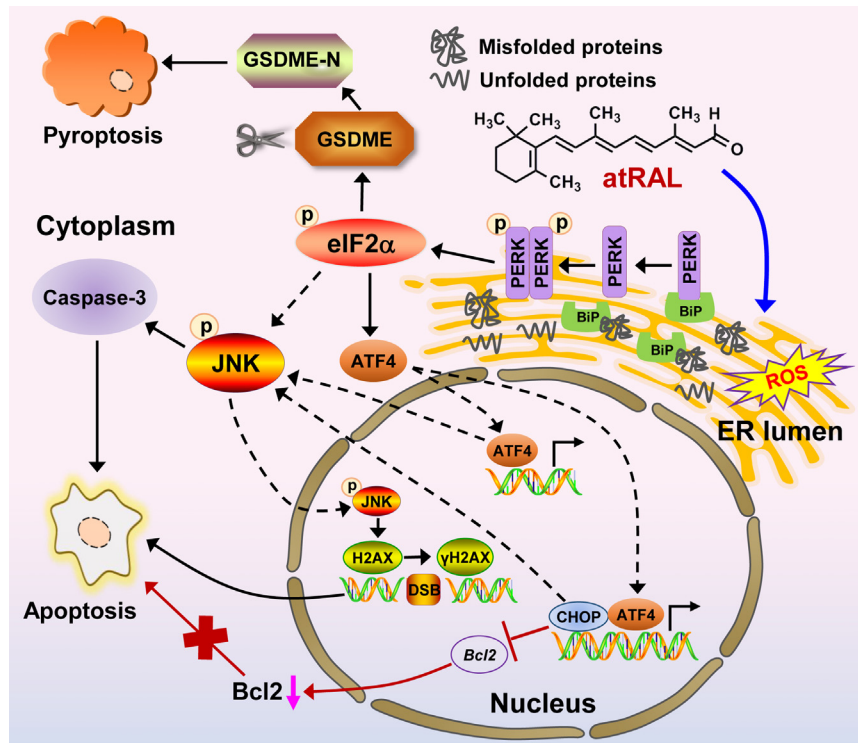


Figure 9. Proposed mechanisms for how activation of eIF2 α by atRAL facilitates photoreceptor and RPE cell death. Misfolded or unfolded proteins accumulate in ER lumen when intracellular atRAL impairs ER function at least partially through ROS production, and they compete for binding of PERK to BiP. Once PERK is dissociated from BiP, it undergoes oligomerization and autophosphorylation and then evokes the phosphorylation of eIF2 α . Active eIF2 α activates JNK signaling both independent of and dependent on ATF4 and the ATF4/CHOP axis, thereby promoting apoptotic cell death through inducing caspase-3 activation and DNA damage. Some p-JNK proteins move into the nucleus where they phosphorylate the histone H2AX to generate DNA DSB marker γ H2AX, indicative of the occurrence of DNA damage. Induction of apoptosis by CHOP is due to JNK activation rather than inhibition of the expression of anti-apoptotic gene *Bcl2*. On the other hand, eIF2 α activation induces the cleavage of GSDME to produce GSDME-N, thus eliciting pyroptotic cell death. atRAL, all-*trans*-retinal; ATF4, activating transcription factor 4; BiP, binding immunoglobulin protein; eIF2 α , eukaryotic translation initiation factor 2 α ; ER, endoplasmic reticulum; JNK, Jun N-terminal kinase; PERK, protein kinase RNA-like ER kinase; ROS, reactive oxygen species.

donkey anti-rabbit (catalog no. A21207) IgG (H + L) secondary antibodies were purchased from Invitrogen. Rabbit anti- γ H2AX (catalog no. NB100–384) was obtained from Novus Biologicals. Rabbit anti-Lamin B1 (catalog no. 12987-1-AP) was purchased from Proteintech Biotechnologies. Cytoplasmic and nuclear extraction kit (catalog no. 78833) and horseradish peroxidase-conjugated goat anti-mouse (catalog no. 31430) and goat anti-rabbit (catalog no. 31460) IgG (H + L) secondary antibodies were purchased from Thermo Fisher Scientific. H&E staining kit (catalog no. P032IH) was obtained from Auragene Biotech. H2DCFDA, Lipofectamine RNAiMAX, and Lipofectamine LTX & PLUS reagents were purchased from Thermo Fisher Scientific. ReverTra Ace qPCR RT Master Mix was obtained from TOYOBO Bio-Technology. PrimeSTAR HS (Premix) (catalog no. R040A) was provided by Takara Biomedical Technology. FastStart Essential DNA Green Master was provided by Roche Applied Science. *Escherichia coli* DH5 α was purchased from Transgene Biotech.

Animals

Abca4^{-/-}*Rdh8*^{-/-} mice on a C57BL/6J genetic background, which do not contain *rd8* mutation in the *Crb1* gene, were generated as we described (17). C57BL/6J WT mice were provided by the Xiamen University Laboratory Animal Center. The protocols for all animal experiments were approved by the

Institutional Animal Care and Use Committee of Xiamen University School of Medicine. *Abca4*^{-/-}*Rdh8*^{-/-} and C57BL/6J WT mice aged 4 weeks were dark adapted for 2 days and then illuminated for 2 h by 10,000-lx LED light. Eyeballs were collected at day 5 after light exposure. Control mice were kept for 7 days in the dark without exposure to light. Alternatively, *Abca4*^{-/-}*Rdh8*^{-/-} mice at 4 weeks of age were dark adapted for 2 days and then injected intraperitoneally with Sal or dimethyl sulfoxide (DMSO) (vehicle) at a dose of 8 mg/kg body weight. Two hours later, the mice were illuminated with 10,000-lx LED light for 2 h, followed by once-daily injection of Sal or DMSO for 4 days. Control *Abca4*^{-/-}*Rdh8*^{-/-} mice were intraperitoneally administered with Sal or DMSO without light exposure.

Rpe65 gene variation genotyping

After the tails of *Abca4*^{-/-}*Rdh8*^{-/-} mice were digested at 65 °C for 16 h, genome DNA was extracted using a genomic DNA kit according to the manufacturer's instruction, followed by amplification with PCR. The variation in the gene *Rpe65* was identified by genome sequencing of the PCR products.

Cell culture

Murine photoreceptor cell line 661W was purchased from Shanghai Zishi Biotechnology. Cells were routinely cultured in

eIF2α promotes retinal degeneration

Dulbecco's modified Eagle's medium (DMEM) (Gibco) supplemented with 10% fetal bovine serum (FBS) (HyClone) and 1% penicillin/streptomycin (Thermo Fisher Scientific) in a humidified incubator with 5% CO₂ at 37 °C.

Treatment with Sal or NAC

Cells were preincubated with 100-μM Sal or 2-mM NAC for 2 h, followed by treatment with 5-μM atRAL for 6 h.

Detection of the localization of intracellular ROS to the ER

661W photoreceptor cells seeded into 6-well plates were cultured overnight. Next, cells were treated with 5-μM atRAL for 6 h and then incubated with 10-μM H2DCFDA, 1-μM ER-tracker Red and 10-μM Hoechst 33,342 at 37 °C for 10 min. After being washed with PBS three times, 1-ml FBS-free DMEM was added into each well, and living cells were imaged by a Zeiss LSM 880+airy scan confocal microscope (Carl Zeiss).

Quantitative real-time PCR

Total cellular RNA was extracted using TRIeasy total RNA extraction reagent. Concentration, purity, and integrity of total RNA were determined by NanoDrop One (Thermo Fisher Scientific). One-μg RNA was reverse transcribed into complementary DNA using ReverTra Ace qPCR RT Master Mix following the manufacturer's protocol. qRT-PCR was performed on a LightCycler 96 instrument (Roche Applied Science) using the FastStart Essential DNA Green Master. Primer sequences are available in Table 1.

RNA interference assay

Cells seeded into 6-well plates (1.5 × 10⁵ cells/well) were cultured overnight and then transfected with 20-μM siRNA specific for *eIF2α* or *Atf4* (1.5 μl/well) using the Lipofectamine RNAiMAX reagent (9 μl/well) according to the manufacturer's instruction. Cells, 24 h after transfection, were treated with 5-μM atRAL for 6 h. Alternatively, cells seeded into 96-well plates at a density of 1 × 10⁴ cells/well were transfected with 20-μM siRNA targeting *eIF2α* (0.3 μl/well) for 24 h using the Lipofectamine RNAiMAX reagent (1.8 μl/well). Then cells were incubated with 5-μM atRAL for 6 h. The siRNA sequences of *eIF2α*, *Atf4*, and NC were shown in Table 2.

Measurement of intracellular Fe²⁺

661W photoreceptor cells seeded into 6-chamber 35-mm glass bottom dishes were transfected with *eIF2α* siRNA

(si*eIF2α*) or NC siRNA for 24 h and then incubated with 5-μM atRAL and DMSO alone for 6 h, respectively. Next, cells were exposed to 5-μM FeRhoNox-1 and 10-μM Hoechst 33,342 for 40 min at 37 °C. After being washed three times with PBS, 1-ml FBS-free DMEM was added into each chamber and living cells were imaged by a Zeiss LSM 780-2 confocal microscope. The fluorescence intensity reflecting Fe²⁺ levels was quantified by ImageJ software (National Institutes of Health).

CRISPR/Cas9 technology

To establish *Chop*^{-/-} 661W photoreceptor cell line, a target sequence in the fourth exon of mouse *Chop* (GCGGGCTCTGATCGACCGCA) was designed at Massachusetts Institute of Technology (<http://crispr.mit.edu>). The primers for the specific guide RNA, which were presented in Table 3 and synthesized by Sangon Biotech, were annealed to form a guide RNA duplex and then cloned into the BsmBI site of pL-CRISPR.EFS.GFP vector purchased from Addgene. The targeting vector was transfected into 661W photoreceptor cells seeded into 6-well plates (2 × 10⁵ cells/well) using the Lipofectamine LTX & PLUS reagent according to the manufacturer's instruction. After 24 h post-transfection, GFP-positive live cells were sorted into single clones using a MoFlo Astrios flow cytometry (Beckman Coulter). Single cells were cultured in 96-well plates for 2 weeks. WT or *Chop*^{-/-} 661W photoreceptor cells seeded into 96- or 6-well plates were cultured overnight and then incubated with 5-μM atRAL for 6 h. *Chop*^{-/-} 661W photoreceptor cells were identified by Western blotting when exposed to atRAL. Cellular morphology was examined by a Leica DM2500 microscope.

Immunofluorescence staining

Cells seeded on cover slips in 24-well plates were incubated with 5-μM atRAL for 6 h and then exposed for 6 h to 5-μM atRAL. After being fixed in 4% paraformaldehyde at 4 °C for 15 min, cells were permeabilized by 0.2% Triton X-100 in PBS for 20 min and then immersed in 2% bovine serum albumin for 1 h to abolish the nonspecific binding at room temperature. Next, cells were incubated with anti-p-PERK antibody (1:100 dilution) at 4 °C overnight followed by incubation with Alexa Fluor 594-conjugated donkey anti-rabbit secondary antibody (1:100 dilution) for 2 h at room temperature. Alternatively, sections of neural retina tissues from mouse eyeballs were incubated at 4 °C overnight with primary antibodies directed against p-PERK, p-JNK, and CHOP (1:100 dilution) and then exposed for 2 h to Alexa Fluor 594-conjugated donkey anti-rabbit (1:100 dilution) secondary antibody at room

Table 1
Primer sequences

Gene	Forward primer	Reverse primer
BiP (<i>Gbp78</i>)	TGTGTGTGAGACCAGAACCG	TAGGTGGTCCCAAGTCGAT
<i>eIF2α</i>	AAGCATGCAGTCTCAGACCC	CTGTGGGGTCAAACGCCTA
<i>Atf4</i>	CCTATAAAGGCTTGCGGCCA	GTCCGTTACAGCAACACTGC
<i>Chop</i>	TCTTGAGCCTAACACGTCGATT	ACGTGGACCAGGTTCTCTCT
<i>Actb</i>	AGATCAAGATCATGCTCCCTC	GGACTGTTACTGAGCTGCGT
<i>Rpe65</i>	TGCATACGGCACTTGGGTTGA	TTCTGGTGCAGTCCCAATCAGT

ATF4, activating transcription factor 4; BiP, binding immunoglobulin protein; *eIF2α*, eukaryotic translation initiation factor 2α.

Table 2
siRNA sequences

Gene	Sence	Antisence
<i>elf2α</i>	GCCCAAAGUGGUCA CAGAUTT	AUCUGUGACCACUUU GGGCTT
<i>Atf4</i>	CCACUCCAGAGCAUU CCUUTT	AAGGAAUGCUCUGGA GUGGTT
NC	UUCUCCGAACGUGUCA CGUTT	ACGUGACACGUUCGG AGAATT

ATF4, activating transcription factor 4; eIF2 α , eukaryotic translation initiation factor 2 α ; NC, negative control.

temperature. Slides were mounted with DAPI in 50% glycerin. Photographs were acquired by an Olympus FV1000 confocal microscope.

Determination of tight junctions in the RPE

Mouse eyeballs were fixed in 4% paraformaldehyde for 30 min at room temperature. Posterior eyecups containing RPE/choroids were carefully collected and then penetrated with 1% Triton X-100 for 1 h, followed by incubation in PBS containing 5% bovine serum albumin and 0.3% Triton X-100 for 1 h. RPE/choroid flat mounts were stained with a mouse monoclonal antibody against ZO-1 at a dilution of 1:100 overnight at 4 °C, and after being washed by PBS three times, they were incubated with an Alexa Fluor 488-conjugated donkey anti-mouse IgG (H + L) secondary antibody (1:200 dilution) for 2 h. Images were captured by the Olympus FV1000 confocal microscope.

Western blotting

Neural retinas were dissected from mouse eyeballs. Western blot analysis of extracts from cells or neural retina tissues was carried out as we described (17). Equal amounts of protein were subjected to electrophoresis in 12% SDS-polyacrylamide gels and transferred to polyvinylidene difluoride membranes (Roche Applied Science). The membranes, 1 h after being blocked with 5% skim milk at room temperature, were incubated with primary antibodies (1: 1000 dilution) specific for BiP, p-eIF2 α , eIF2 α , ATF4, CHOP, p-JNK, JNK, p-c-Jun, c-Jun, cleaved caspase-3, PARP, γ H2AX, GSDME, Lamin B1, GAPDH, or β -actin at 4 °C overnight, followed by incubation with the corresponding secondary antibodies (1: 5000 dilution) for 1 h at room temperature. Blots were imaged on a ChemiDoc XRS+ Imaging system (Bio-Rad) by using electrochemiluminescence Western blotting detection reagents (Advansta). Band intensities were quantified by densitometry using ImageJ software. Unprocessed original images of gels, in which boxes in *red* indicated selected Western blot results, were shown in Fig. S3.

Table 3
Guide RNA sequences

Gene	Forward primer	Reverse primer
<i>Chop</i>	CACCGCGGGCTCT GATCGACCGCA	AAACTGCGGTTCGATCA GAGCCCGC

TUNEL staining assay

After dewaxing and rehydration, the paraffin sections of mouse neural retina were fixed in 4% paraformaldehyde at 4 °C for 15 min and then washed with PBS three times. Apoptosis was detected by TUNEL assay kit (Promega) according to the manufacturer's instruction. The resulting slides were stained with DAPI, followed by examination with the Olympus FV1000 confocal microscope.

H&E staining

The eyeballs of mice were fixed in formaldehyde, acetic acid, and saline fixative solution (Servicebio) at 4 °C for 24 h and then embedded in paraffin. Sections at the thickness of 3 microns were cut from paraffin-embedded tissues and routinely stained with H&E. Photographs were taken with the Leica DM2500 microscope.

Fundus imaging

Mice were anesthetized with 200 μ l of 1% pentobarbital sodium by intraperitoneal injection and their pupils were dilated with 1% tropicamide. To prevent cataract formation and keep the cornea surface clarified and hydrated, a drop of 0.2% carbomer solution was placed into mouse eyes. Fundus images of the mice were captured by a small animal retinal imaging system (Optoprobe; OPIMG-L).

Separation of the nuclear fraction

Cells were harvested with 0.25% trypsin-EDTA after treatment with atRAL for 6 h and then centrifuged at 500g for 5 min at 4 °C. Cell pellets were suspended in prechilled PBS, followed by centrifugation at 4 °C for 3 min. Following the removal of the supernatant, the residue was completely dried. The nuclear fraction was extracted using a cytoplasmic and nuclear extraction kit from Thermo Fisher Scientific in accordance with the manufacturer's protocol. Finally, the resulting samples were subjected to Western blot analysis.

Statistical analyses

Data were analyzed using GraphPad Prism software (Version 8.0) and shown as the mean \pm SD of at least three independent experiments. Statistical analyses were performed by Student's *t* test or one-way or two-way ANOVA followed by Tukey's multiple comparison test or Bonferroni's multiple comparison test, as indicated in corresponding figure legends. In all cases, *p*-values below 0.05 were considered statistically significant.

Data availability

The data supporting the findings of this study are available within the article and the supporting information.

Supporting information—This article contains Supporting information.

Author contributions—Y. Wu. conceptualization; D. H., Z. L., and Y. Wu. methodology; D. H., L. T., B. C., C. L., Y. C., and Y. Wu.

eIF2 α promotes retinal degeneration

investigation; D. H., X. C., Y. Wang, S. L., J. C., and Y. Wu formal analysis; D. H., C. L., and Y. Wu. writing-original draft; Y. Wu. funding acquisition; Y. Wu. project administration; Y. Wu. resources; D. H., L. T., B. C., X. C., Y. Wang, S. L., C. L., Y. C., J. C., Z. L., and Y. Wu. writing-review and editing.

Funding and additional information—This work was supported by National Natural Science Foundation of China grants 82,171,064 and 81,870,671 (to Y. Wu.), Guangdong Basic and Applied Basic Research Foundation grants 2022A1515012514 and 2021A1515011391 (to Y. Wu.), and the Open Innovation Fund for undergraduate students of Xiamen University.

Conflicts of interest—The authors declare that they have no competing conflicts of interest with the contents of this article.

Abbreviations—The abbreviations used are: AMD, age-related macular degeneration; ATF4, activating transcription factor 4; atRAL, all-trans-retinal; BiP, binding immunoglobulin protein; DAPI, 4',6-diamidino-2-phenylindole; DMEM, Dulbecco's modified Eagle's medium; DMSO, dimethyl sulfoxide; eIF2 α , eukaryotic translation initiation factor 2 α ; ER, endoplasmic reticulum; FBS, fetal bovine serum; H2DCFDA, 2',7'-dichlorodihydrofluorescein diacetate; JNK, Jun N-terminal kinase; LED, light emitting diode; NAC, N-acetyl-L-cysteine; NC, negative control; PARP, Poly ADP-ribose polymerase; PERK, protein kinase RNA-like ER kinase; qRT-PCR, quantitative real-time PCR; RDH8, retinol dehydrogenase 8; ROS, reactive oxygen species; STGD1, Stargardt's disease; UPR, unfolded protein response.

References

1. Saari, J. C. (2012) Vitamin A metabolism in rod and cone visual cycles. *Annu. Rev. Nutr.* **32**, 125–145
2. Kiser, P. D., and Palczewski, K. (2016) Retinoids and retinal diseases. *Annu. Rev. Vis. Sci.* **2**, 197–234
3. Liu, X., Chen, J., Liu, Z., Li, J., Yao, K., and Wu, Y. (2016) Potential therapeutic agents against retinal diseases caused by aberrant metabolism of retinoids. *Invest. Ophthalmol. Vis. Sci.* **57**, 1017–1030
4. Tsybovsky, Y., Molday, R. S., and K, P. (2010) The ATP-binding cassette transporter ABCA4: Structural and functional properties and role in retinal disease. *Adv. Exp. Med. Biol.* **703**, 105–125
5. Rattner, A., Smallwood, P. M., and Nathans, J. (2000) Identification and characterization of all-trans-retinol dehydrogenase from photoreceptor outer segments, the visual cycle enzyme that reduces all-trans-retinal to all-trans-retinol. *J. Biol. Chem.* **275**, 11034–11043
6. Allikmets, R., Singh, N., Sun, H., Shroyer, N. F., Hutchinson, A., Chidambaram, A., et al. (1997) A photoreceptor cell-specific ATP-binding transporter gene (ABCR) is mutated in recessive Stargardt macular dystrophy. *Nat. Genet.* **15**, 236–246
7. Rivera, A., White, K., Stöhr, H., Steiner, K., Hemmrich, N., Grimm, T., et al. (2000) A comprehensive survey of sequence variation in the ABCA4 (ABCR) gene in Stargardt disease and age-related macular degeneration. *Am. J. Hum. Genet.* **67**, 800–813
8. Cremers, F., Lee, W., Collin, R., and Allikmets, R. (2020) Clinical spectrum, genetic complexity and therapeutic approaches for retinal disease caused by ABCA4 mutations. *Prog. Retin. Eye Res.* **79**, 100861
9. Allikmets, R., Shroyer, N. F., Singh, N., Seddon, J. M., Lewis, R. A., Bernstein, P. S., et al. (1997) Mutation of the Stargardt disease gene (ABCR) in age-related macular degeneration. *Science* **277**, 1805–1807
10. Allikmets, R. (2000) Further evidence for an association of ABCR alleles with age-related macular degeneration. The International ABCR Screening Consortium. *Am. J. Hum. Genet.* **67**, 487–491
11. Zhang, R., Wang, L. Y., Wang, Y. F., Wu, C. R., Lei, C. L., Wang, M. X., et al. (2015) Associations of the G1961E and D2177N variants in ABCA4 and the risk of age-related macular degeneration. *Gene* **567**, 51–57
12. Souied, E. H., Ducroq, D., Rozet, J. M., Gerber, S., Perrault, I., Munnich, A., et al. (2000) ABCR gene analysis in familial exudative age-related macular degeneration. *Invest. Ophthalmol. Vis. Sci.* **41**, 244–247
13. Maeda, A., Maeda, T., Imanishi, Y., Kuksa, V., Alekseev, A., Bronson, J. D., et al. (2005) Role of photoreceptor-specific retinol dehydrogenase in the retinoid cycle *in vivo*. *J. Biol. Chem.* **280**, 18822–18832
14. Maeda, A., Maeda, T., Golczak, M., and Palczewski, K. (2008) Retinopathy in mice induced by disrupted all-trans-retinal clearance. *J. Biol. Chem.* **283**, 26684–26693
15. Maeda, A., Maeda, T., Golczak, M., Chou, S., Desai, A., Hoppel, C. L., et al. (2009) Involvement of all-trans-retinal in acute light-induced retinopathy of mice. *J. Biol. Chem.* **284**, 15173–15183
16. Chen, Y., Okano, K., Maeda, T., Chauhan, V., Golczak, M., Maeda, A., et al. (2012) Mechanism of all-trans-retinal toxicity with implications for Stargardt disease and age-related macular degeneration. *J. Biol. Chem.* **287**, 5059–5069
17. Liao, C., Cai, B., Feng, Y., Chen, J., Wu, Y., Zhuang, J., et al. (2020) Activation of JNK signaling promotes all-trans-retinal-induced photoreceptor apoptosis in mice. *J. Biol. Chem.* **295**, 6958–6971
18. Chen, C., Chen, J., Wang, Y., Liu, Z., and Wu, Y. (2021) Ferroptosis drives photoreceptor degeneration in mice with defects in all-trans-retinal clearance. *J. Biol. Chem.* **296**, 100187
19. Cai, B., Liao, C., He, D., Chen, J., Han, J., Lu, J., et al. (2022) Gasdermin E mediates photoreceptor damage by all-trans-retinal in the mouse retina. *J. Biol. Chem.* **298**, 101553
20. Braakman, I., and Bulleid, N. J. (2011) Protein folding and modification in the mammalian endoplasmic reticulum. *Annu. Rev. Biochem.* **80**, 71–99
21. Ron, D., and Walter, P. (2007) Signal integration in the endoplasmic reticulum unfolded protein response. *Nat. Rev. Mol. Cell Biol.* **8**, 519–529
22. Hetz, C., Zhang, K., and Kaufman, R. J. (2020) Mechanisms, regulation and functions of the unfolded protein response. *Nat. Rev. Mol. Cell Biol.* **21**, 421–438
23. Hetz, C., Lee, A. H., Gonzalez-Romero, D., Thielen, P., Castilla, J., Soto, C., et al. (2008) Unfolded protein response transcription factor XBP-1 does not influence prion replication or pathogenesis. *Proc. Natl. Acad. Sci. U. S. A.* **105**, 757–762
24. Hiramatsu, N., Chiang, K., Aivati, C., Rodvold, J. J., Lee, J. M., Han, J., et al. (2020) PERK-mediated induction of microRNA-483 disrupts cellular ATP homeostasis during the unfolded protein response. *J. Biol. Chem.* **295**, 237–249
25. Hughes, D., and Mallucci, G. R. (2019) The unfolded protein response in neurodegenerative disorders—therapeutic modulation of the PERK pathway. *FEBS J.* **286**, 342–355
26. Cui, W., Li, J., Ron, D., and Sha, B. (2011) The structure of the PERK kinase domain suggests the mechanism for its activation. *Acta Crystallogr. D Biol. Crystallogr.* **67**, 423–428
27. Harding, H. P., Zhang, Y., Bertolotti, A., Zeng, H., and Ron, D. (2000) Perk is essential for translational regulation and cell survival during the unfolded protein response. *Mol. Cell* **5**, 897–904
28. Carrara, M., Prischi, F., Nowak, P. R., and Ali, M. M. (2015) Crystal structures reveal transient PERK luminal domain tetramerization in endoplasmic reticulum stress signaling. *EMBO J.* **34**, 1589–1600
29. Walter, P., and Ron, D. (2011) The unfolded protein response: from stress pathway to homeostatic regulation. *Science* **334**, 1081–1086
30. Hetz, C., Chevet, E., and Oakes, S. A. (2015) Proteostasis control by the unfolded protein response. *Nat. Cell Biol.* **17**, 829–838
31. Tan, E., Ding, X. Q., Saadi, A., Agarwal, N., Naash, M. I., and Al-Ubaidi, M. R. (2004) Expression of cone-photoreceptor-specific antigens in a cell line derived from retinal tumors in transgenic mice. *Invest. Ophthalmol. Vis. Sci.* **45**, 764–768
32. Lee, A. S. (2005) The ER chaperone and signaling regulator GRP78/BiP as a monitor of endoplasmic reticulum stress. *Methods* **35**, 373–381
33. Cao, S. S., and Kaufman, R. J. (2012) Unfolded protein response. *Curr. Biol.* **22**, R622–R626

34. Dhanasekaran, D. N., and Reddy, E. P. (2008) JNK signaling in apoptosis. *Oncogene* **27**, 6245–6251
35. Lu, C., Zhu, F., Cho, Y. Y., Tang, F., Zykova, T., Ma, W. Y., *et al.* (2006) Cell apoptosis: requirement of H2AX in DNA ladder formation, but not for the activation of caspase-3. *Mol. Cell* **23**, 121–132
36. Mielke, K., and Herdegen, T. (2000) JNK and p38 stresskinases—degenerative effectors of signal-transduction-cascades in the nervous system. *Prog. Neurobiol.* **61**, 45–60
37. Tewari, M., Quan, L. T., O'Rourke, K., Desnoyers, S., Zeng, Z., Beidler, D. R., *et al.* (1995) Yama/ CPP32 beta, a mammalian homolog of CED-3, is a CrmA-inhibitable protease that cleaves the death substrate poly(ADP-ribose) polymerase. *Cell* **81**, 801–809
38. Modesti, M., and Kanaar, R. (2001) DNA repair: spot(light)s on chromatin. *Curr. Biol.* **11**, R229–R232
39. Davis, R. J. (2000) Signal transduction by the JNK group of MAP kinases. *Cell* **103**, 239–252
40. Major, C. D., and Wolf, B. A. (2001) Interleukin-1 β stimulation of c-Jun NH₂-terminal kinase activity in insulin-secreting cells: evidence for cytoplasmic restriction. *Diabetes* **50**, 2721–2728
41. Boyce, M., Bryant, K. F., Jousse, C., Long, K., Harding, H. P., Scheuner, D., *et al.* (2005) A selective inhibitor of eIF2 α dephosphorylation protects cells from ER stress. *Science* **307**, 935–939
42. Marciniak, S. J., Yun, C. Y., Oyadomari, S., Novoa, I., Zhang, Y., Jungreis, R., *et al.* (2004) CHOP induces death by promoting protein synthesis and oxidation in the stressed endoplasmic reticulum. *Genes Dev.* **18**, 3066–3077
43. Luitl, V., Isas, J. M., Kaye, R., Glabe, C. G., Langen, R., and Chen, J. (2006) Drusen deposits associated with aging and age-related macular degeneration contain nonfibrillar amyloid oligomers. *J. Clin. Invest.* **116**, 378–385
44. Kamalden, T. A., Hiscott, P., Jackson, M., and Grierson, I. (2020) Secretory proteostasis of the retinal pigmented epithelium: impairment links to age-related macular degeneration. *Prog. Retin. Eye Res.* **79**, 100859
45. Li, J., Cai, X., Xia, Q., Yao, K., Chen, J., Zhang, Y., *et al.* (2015) Involvement of endoplasmic reticulum stress in all-*trans*-retinal-induced retinal pigment epithelium degeneration. *Toxicol. Sci.* **143**, 196–208
46. Hamamura, K., Lin, C. C., and Yokota, H. (2013) Salubrinal reduces expression and activity of MMP13 in chondrocytes. *Osteoarthr. Cartilage* **21**, 764–772
47. Li, Y., Jiang, W., Niu, Q., Sun, Y., Meng, C., Tan, L., *et al.* (2019) eIF2 α -CHOP-BCL-2/JNK and IRE1 α -XBP1/JNK signaling promote apoptosis and inflammation and support the proliferation of Newcastle disease virus. *Cell Death Dis* **10**, 891
48. Tabas, I., and Ron, D. (2011) Integrating the mechanisms of apoptosis induced by endoplasmic reticulum stress. *Nat. Cell Biol.* **13**, 184–190
49. Morton, S., Davis, R. J., McLaren, A., and Cohen, P. (2003) A reinvestigation of the multisite phosphorylation of the transcription factor c-Jun. *EMBO J.* **22**, 3876–3886
50. Liao, Y., Zhang, H., He, D., Wang, Y., Cai, B., Chen, J., *et al.* (2019) Retinal pigment epithelium cell death is associated with NLRP3 inflammasome activation by all-*trans* retinal. *Invest. Ophthalmol. Vis. Sci.* **60**, 3034–3045
51. Tao, L., He, D., Liao, C., Cai, B., Chen, C., Wang, Y., *et al.* (2022) Repressing c-Jun N-terminal kinase signaling mitigates retinal pigment epithelium degeneration in mice with failure to clear all-*trans*-retinal. *Exp. Eye Res.* **214**, 108877